Organic Electronics 15 (2014) 692–700

Contents lists available at ScienceDirect

Organic Electronics

journal homepage: www.elsevier.com/locate/orgel

Organic photovoltaic devices incorporating a molybdenum oxide hole-extraction layer deposited by spray-coating from an ammonium molybdate tetrahydrate precursor

Jonathan Griffin, Andrew J. Pearson, Nicholas W. Scarratt, Tao Wang, David G. Lidzey *, Alastair R. Buckley *

Department of Physics & Astronomy, University of Sheffield, S3 7RH, UK

ARTICLE INFO

Article history:
Received 28 October 2013
Received in revised form 17 December 2013
Accepted 24 December 2013
Available online 7 January 2014

Keywords:
Organic photovoltaics
Molybdenum oxide
Spray coating
PCDTBT
Polymer

ABSTRACT

Polymer bulk heterojunction solar cells have been constructed using a thin film molybdenum oxide (MoOx) hole extraction layer that was fabricated by thermally annealing an ammonium molybdate tetrahydrate precursor layer deposited in air by ultrasonic spray-coating. Onto this layer was spray cast a PCDTBT:$PC_{71}BM$ film that acted as the active light-harvesting and charge-transporting layer. We optimise the processing steps used to convert the spray-cast MoOx precursor and show that the temperature at which it is annealed is critical to achieving high device efficiency as it both facilitates the removal of trapped solvent as well as driving its chemical conversion to MoOx. We demonstrate that by optimising the spray-casting and annealing process, we are able to create solar cell devices having a peak power conversion efficiency of 4.4%.

1. Introduction

The manufacturing and materials costs of solar cells provide barriers to the growth in the adoption of photovoltaic electricity generation, and limit the returns on investment in generation capacity. Polymer organic cells still promise potential significant cost reductions through the possibility of high volume, low temperature and vacuum-less cell processing by roll-to-roll processing [1]. In order for polymer organic photovoltaic cells to become commercially viable, improvements in the manufacturability, efficiency and lifetime of devices need to be achieved [2]. Rapid improvements in the power conversion efficiency (PCE) of organic photovoltaic (OPV) devices have been seen, with single junction OPVs now exceeding 9% [3]. This has in part been due to a better understanding of the properties required by donor and acceptor materials in order to achieve high efficiencies and also the ability to synthesise these required materials [4,5]. Currently new donor materials such as Poly[N-9′-heptadecanyl-2,7-carbazole-alt-5,5-(4′,7′-di-2-thienyl-2′,1′,3′-benzothiadiazole)] (PCDTBT) and similar derivatives are being synthesised with properties close to that of an ideal donor [4,6,7]. However many of these new donors differ from older materials such as poly(3-hexylthiophene-2,5-diyl) (P3HT) in the fact that their highest occupied molecular orbitals (HOMOs) are deeper [4,7,8]. This general increase in the depth of the HOMO level has required the development of new electrode materials to facilitate the efficient extraction of holes from materials such as PCDTBT [9,10]. One such electrode modification material is the metal oxide molybdenum oxide [11,12]. We henceforth refer to molybdenum oxide as MoOx as the molybdenum in thin films of this material can exist in a variety of different oxidation states.

At present, most OPV devices fabricated in a research environment have been created using deposition

* Corresponding authors. Tel.: +44 0114 222 3501; fax: +44 0114 222 3555 (D.G. Lidzey).
E-mail addresses: D.G.Lidzey@sheffield.ac.uk (D.G. Lidzey), alastair.buckley@sheffield.ac.uk (A.R. Buckley).

1566-1199/$ - see front matter © 2014 Elsevier B.V. All rights reserved.
http://dx.doi.org/10.1016/j.orgel.2013.12.028

techniques such as spin coating from solution or vacuum based deposition techniques to deposit both the active semiconducting and hole extracting interfacial layers [11–13]. Whilst spin-coating is a high-precision technique that permits films to be fabricated having excellent uniformity and control over thickness, it is not compatible with high-volume manufacturing processes. Recently, attention has turned to the use of spray-coating to deposit materials for organic-electronics. Ultrasonic spray-coating is a solution based deposition technique that is easily scalable and has been shown to be able to deposit organic active layers within OPVs while retaining high efficiencies [14–18]. Spray-coating has also been used to deposit the hole-extracting polymer PEDOT:PSS [19], with spray-pyrolysis (a technique in which precursor solutions are sprayed onto a preheated substrate) being used to deposit metal oxide films [20]. There appears therefore to be significant scope to explore the application of spray-based techniques to deposit a range of functional materials for thin-film electronics applications, as a number of groups have shown that metal oxide films can be prepared from solution via a range of precursors [21–24]. Many of such processes require thermal annealing to convert the precursor into the metal-oxide, although the precursor ammonium molybdate tetrahydrate ($(NH_4)_6Mo_7O_{24}{\cdot}4H_2O$) can also be initially converted to MoOx *in solution* by heating, with the aqueous solutions being cast to form a MoOx film [25]. Notably however such thin films still require thermal annealing; a process that is presumably necessary to remove adsorbed water.

Here, we report the fabrication of OPVs using the sequential deposition of a metal oxide hole extraction layer and an active semiconductor layer with both layers deposited by ultrasonic spray-coating. To fabricate a MoOx hole extraction layer, we have used the precursor material ammonium molybdate tetrahydrate ($(NH_4)_6Mo_7O_{24}{\cdot}4H_2O$) that was then thermally annealed to convert it to MoOx. We characterise the various films using X-ray photoelectron spectroscopy (XPS), ultraviolet photoelectron spectroscopy (UPS), spectroscopic ellipsometry and atomic force microscopy (AFM), and discuss their electronic structure, oxidation state, thickness and surface morphology. We also use such films as the hole-extraction layer in OPV devices and comment on device efficiency. We show that by optimising the deposition condition and annealing temperature, we can fabricate spray-cast devices that have a peak (average) power conversion efficiency of 4.4 (4.1)%.

2. Experimental

Ammonium molybdate tetrahydrate (99.98%) was purchased from Sigma Aldrich, chlorobenzene (99.95%) was purchased from Sigma Aldrich. PCDTBT was synthesized according to a previously reported method [7], and had a M_W of 26.5 KDa with a PDI of 2.18. $PC_{71}BM$ was purchased from Ossila Ltd and had a purity of 95% (5% $PC_{61}BM$). Aluminium, calcium and molybdenum oxide pellets (99.95% purity) were purchased from Testbourne Ltd.

Samples for use in XPS, UPS and AFM were prepared on unpatterened indium tin oxide (ITO) substrates while OPVs were prepared on pre-patterened ITO substrates, (both purchased from Ossila Ltd). Samples for ellipsometry were prepared on a Si ⟨100⟩ wafer. All substrates were cleaned by sonicating in hot deionized (DI) water/Hellmanex, rinsed in DI water followed by hot isopropyl alcohol and then dried using nitrogen gas. Finally, substrates were exposed to a UV-ozone plasma to remove any remaining organic residue from the surface before the deposition of the MoOx precursor layer.

Spray-coating of the MoOx precursor and OPV active layer was performed using a Prism ultra-sonic spray-coater supplied by Ultrasonic Systems Inc. (USI). Fig. 1(a) shows a schematic representation of the spray coating process.

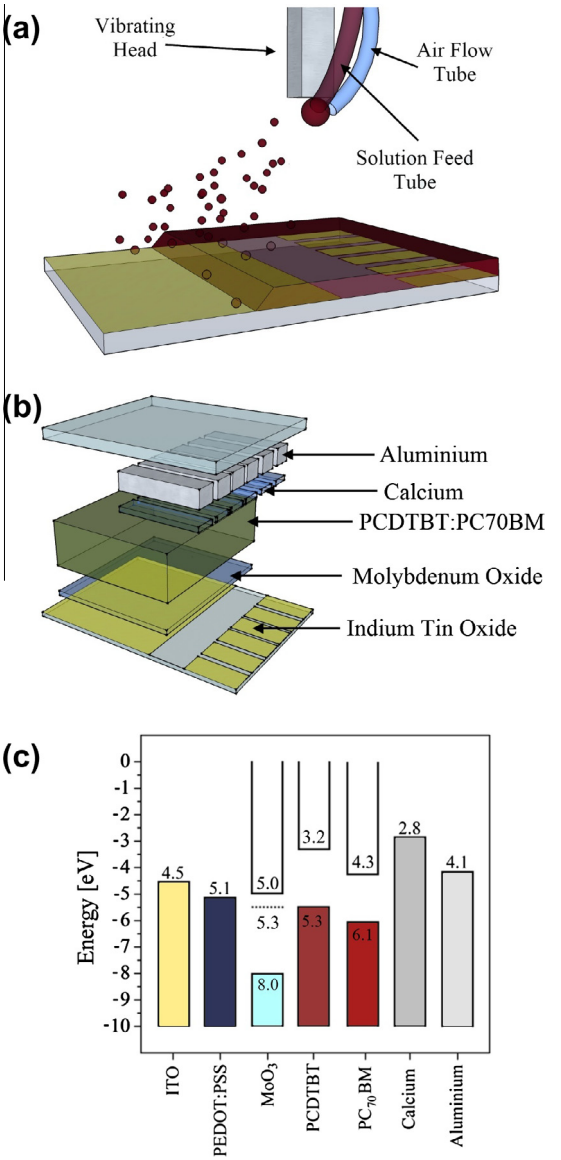

Fig. 1. (a) Schematic representation of the ultrasonic spray coating system, (b) the device architecture where films are deposited onto pre patterned ITO coated substrates, and (c) shows a flat band diagram of the energy levels within standard PCDTBT:$PC_{71}BM$ OPV device.

Ultrasonic spray-coating relies upon the delivery of a solution onto a metallic head that vibrates at 35 kHZ. This causes the solution to disperse into micron-sized droplets that are directed towards a surface of interest using a nitrogen gas stream. In our spray-casting experiments, the ammonium molybdate tetrahydrate was dissolved in high purity DI water at a concentration of 15 mg ml^{-1}. Acetonitrile and DI water were then added to the solution in a ratio of 2:3 DI water to acetonitrile to reduce to solution to a concentration of 6 mg ml^{-1}. The function of the acetonitrile was to reduce the surface tension and viscosity of the solution and thus aid its wetting onto the ITO substrate. The solution was passed through a 0.45 μm PTFE filter and then placed within the ultra-sonic spray-coater. The solution was sprayed from a height of 45 mm above the substrate with a pass speed of 60 mm s^{-1} onto a substrate held at a temperature of 60 °C, forming a 13 nm thick layer. Substrates were then transferred onto a hot plate and annealed at various temperatures in air for 1 min. For comparison, 10 nm MoOx films were also prepared by thermal evaporation at a base pressure of $\sim 10^{-6}$ mbar.

The electronic structure of the various films was explored using X-ray and Ultra-violet photoelectron spectroscopy (XPS and UPS). XPS measurements were performed using a Kratos ultra AXIS photoelectron spectrometer via the Al kα emission line at 1486.6 eV, with the intensity of the Mo3d (225–240 eV), O1s (524–540 eV), N1s (390–412 eV) and C1s (277–298 eV) peaks recorded. C1S peaks were used for calibrating the charging of samples against the position of the peak for adventitious carbon at 284.6 eV. UPS samples were also measured using the Kratos ultra AXIS photoelectron spectrometer using a He(I) emission line at 21.22 eV. Note that as the MoOx and organic semiconductor layers in the OPV devices were spray-cast in air, the samples characterised by UPS/XPS were deliberately exposed to air before measurement to replicate this experimental step.

The structure of the various films fabricated was explored using a Veeco Dimension 3100 AFM operating in tapping mode. Tips from Budget Sensors (300G-Al) were used with a resonance at 300 kHz and a spring constant of 40 N $m-^{1}$. Changes in film thickness during annealing were characterised using a J.A. Woollam Co M2000v spectroscopic ellipsometer over the wavelength range 370–1000 nm. In situ thermal annealing experiments were conducted using a Linkam heating stage and controller with heating and cooling rates of 90 °C min^{-1}. Spectroscopic ellipsometry measurements were acquired every 0.5 s, with film thickness extracted from the raw ellipsometry data via application of a Cauchy model over the wavelength range 700–1000 nm. The uniformity of the spray-cast MoOx films were also characterised over larger areas using a Bruker Contour GT optical interferometer, a 10× magnification and a scan length of 300 μm were used.

The nanostructure of the precursor and MoOx films was characterised using grazing incidence X-ray scattering (GIWAXS) measurements performed at the I07 beam-line at the Diamond Light Source (UK). Samples for measurement on a silicon wafer were positioned inside a custom built experimental chamber filled with helium to reduce scatter, with a Pilatus 2M detector used to collect the scattered X-rays. GIWAXS data was recorded for a range of grazing angles (θ = 0.12°–0.18°), with data presented at the critical angle of 0.18°. Further details of the GIWAXS measurements can be found in Ref. [26].

Spray-cast precursor and annealed MoOx films were used as the hole-extraction layer in organic photovoltaic device. Fig. 1(b) shows the structure of the OPVs explored. The devices were defined between an ITO/MoOx anode and a calcium/aluminium cathode, with both the active organic semiconductor and the hole-extraction layer deposited by spray-coating. The active organic layer was composed of a 60 nm thick 1:4 blend of the low energy-gap donor–acceptor co-polymer PCDTBT together with the fullerene acceptor $PC_{71}BM$. Note that we have previously used optical interferometry to characterise the thickness uniformity a range of polymer:fullerene films deposited by spray-casting over an area of (0.46 × 0.62) mm^2 and find that it to comparable to that obtained using spin-coating [14]. The active layer was deposited from a solution of a PCDTBT:$PC_{71}BM$ dissolved in chlorobenzene with a blend ratio of 1:4 at an overall concentration of 4 mg ml^{-1}. This solution was first passed through a 0.45 μm PVDF filter before spray-coating. The solution was sprayed from a height of 35 mm above the substrate with a pass speed of 80 mm s^{-1} and a substrate temperature of 40 °C. Following this, devices were transferred into a nitrogen filled glovebox for the deposition of the top calcium (3 nm)/aluminium (100 nm) cathode via vacuum evaporation. Deposition was performed in a thermal evaporator at a base pressure of $\sim 10^{-7}$mbar, with the pressure during deposition being $\sim 10^{-6}$mbar. After deposition, the devices were encapsulated under nitrogen using a glass slide fixed in place by an inert UV-setting epoxy. For reference, we plot a flat-band diagram of the device in Fig. 1(c) indicating the line-up of the HOMO and LUMO levels of the PCDTBT and $PC_{71}BM$ with the anode and cathode work-functions [7,25].

The OPV devices fabricated consisted of 6 individual pixels, each having an area of 4.8 mm^2. The JV characteristics of OPV devices were measured under ambient conditions using a Keithley 2400 source meter and a Newport 92251A-1000 AM1.5 solar simulator (power adjusted to 100 mW cm^{-2} at 25 °C using an NREL calibrated silicon diode), with a 4.5 mm^2 shadow mask used to define the illuminated area. From this we determined device performance metrics together with series and shunt resistance calculated from the gradient of the J–V curve at open circuit and short circuit conditions. In our analysis device of device performance, we have selected 50% of pixels with highest efficiency from each deposition condition in order to remove any failed pixels and prevent any selection bias.

3. Results

In Fig. 2(a–d) we plot *FF*, J_{SC}, *PCE* and V_{OC} respectively recorded from OPVs using a spray-cast MoOx precursor film that was annealed at a range of temperatures up to 400 °C. In all cases, the average device metrics together with series and shunt resistance are summarised in Table 1. It can be seen that the OPVs fabricated have a performance and

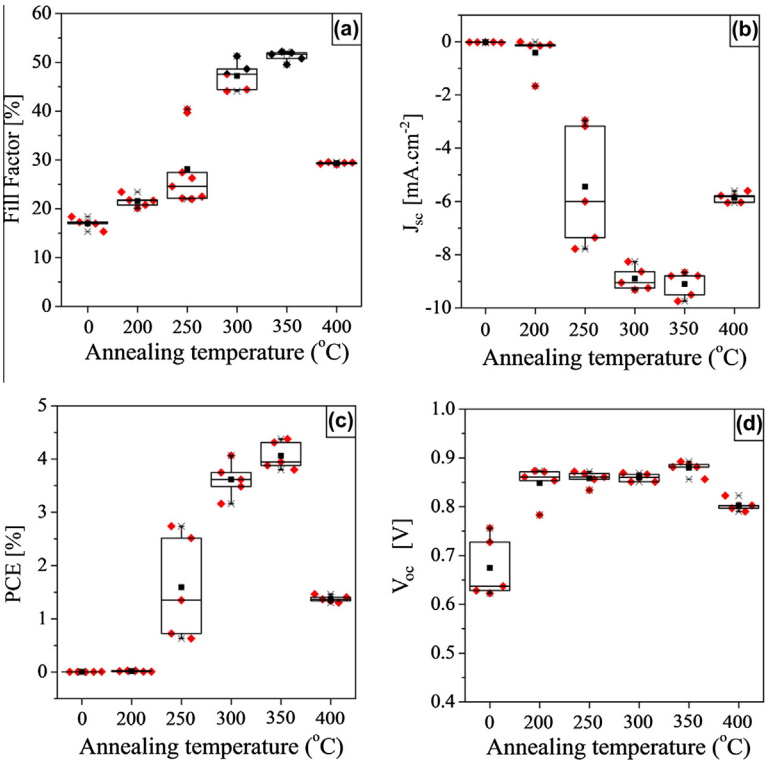

Fig. 2. Device data for OPVs fabricated onto spray-cast ammonium molybdate tetrahydrate films annealed at different temperatures.

Table 1
The average values for the fill factor, open circuit voltage, power conversion efficiency, short circuit current, series and shunt resistances for OPV devices fabricated on ammonium molybdate tetrahydrate layers as a function of annealing temperature.

	FF (%)	V_{oc} (V)	PCE (%)	J_{sc} (mA cm^{-2})	R_S (Ω cm^2)	R_{SH} (Ω cm^2)
Unannealed	17.0	0.67	10^{-2}	−0.01	26,400	16,000
200 °C Anneal	21.8	0.85	10^{-2}	−0.17	2070	3400
250 °C Anneal	28.0	0.86	1.6	−5.45	90	270
300 °C Anneal	47.5	0.86	3.6	−8.92	23	500
350 °C Anneal	51.6	0.88	4.1	−9.12	15	590
400 °C Anneal	29.2	0.80	1.4	−5.86	90	190

efficiency that depends strongly on the annealing temperature used to convert the ammonium molybdate tetrahydrate to MoOx. Indeed, in the device in which the precursor film was not annealed, we observe no measurable photovoltaic response. It can be seen that as the film annealing temperature is raised to 350 °C, the efficiency of the OPV devices increases progressively, reaching a maximum PCE of 4.4% obtained as a result of increasing short circuit current density (J_{sc}) and Fill-Factor (*FF*). This efficiency is in good accord with fully optimised OPVs made in our lab that use a thermally-evaporated MoOx film, a spin-cast PCDTBT:$PC_{71}BM$ active layer and a Ca/Al cathode that have an average efficiency of 4.9% [15]. We find that the series and shunt resistance are a strong-function of annealing temperature, taking maximum values of 26.4 and 16 kΩ cm^2 respectively in the unannealed film; values consistent with a resistive film. On annealing, the series resistance falls, and at 350 °C (corresponding to the annealing temperature at which the device efficiency fill-factor take maximum values) it takes a value of 15 Ω cm^2. On further annealing, series resistance rises to 90 Ω cm^2. The behaviour of the shunt resistance is more complicated; on annealing to 250 °C it falls to 90 Ω cm^2 but then rises to 590 Ω cm^2 on annealing at 350 °C as the fill-factor increases. On annealing to 400 °C, the shunt resistance falls to 190 Ω cm^2 consistent with the reduced fill-factor of 29.2%.

To explore the effect of annealing temperature on the ammonium molybdate tetrahydrate, photoelectron spectroscopy was used to study its chemical composition and electronic structure. In Fig. 3a and b, we plot the Mo3*d* and N1*s* XPS spectra respectively recorded from spray-cast ammonium molybdate tetrahydrate films that are either (i) as cast, or annealed at (ii) 200 °C, (iii) 300 °C or (iv) 400 °C. We also summarise the relative fraction of molybdenum detected in Mo^{5+} and Mo^{6+} oxidation states in Table 2. Here, it can be seen that the reduced Mo^{5+} state is only detected in significant quantities in films that have been

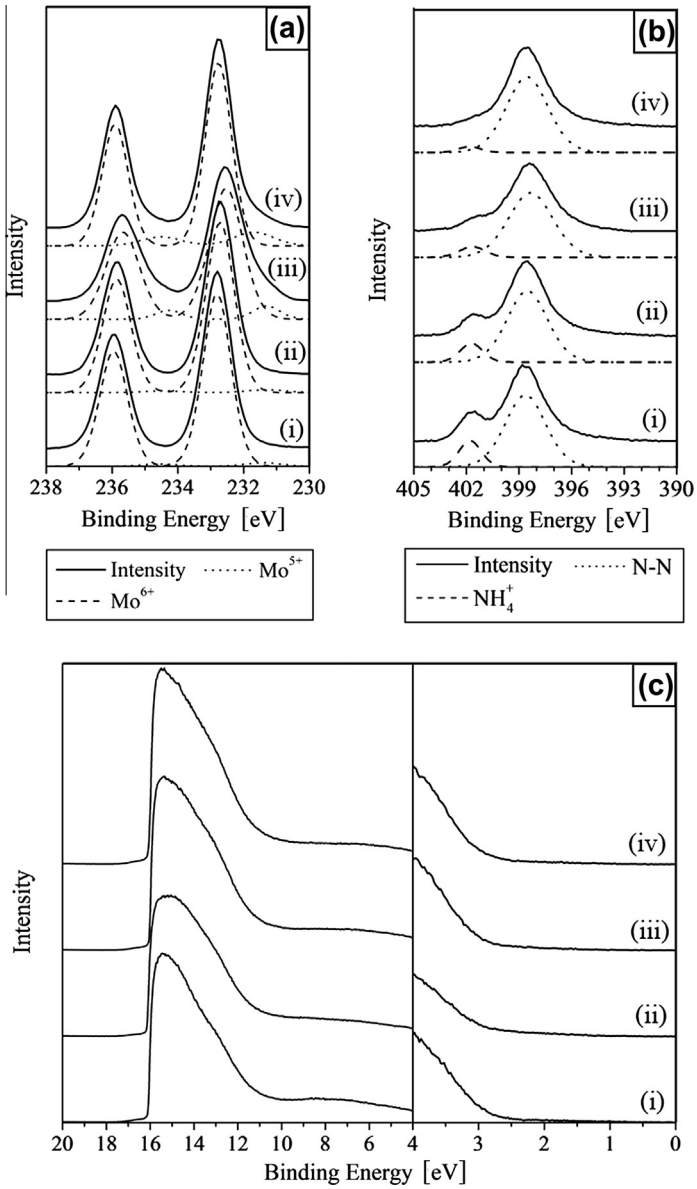

Fig. 3. Photoelectron spectra of (a) the Mo3d peak, (b) the N1s peak, and (c) the UPS spectra for spray-cast ammonium molybdate tetrahydrate films with (i) no annealing, and annealed at (ii) 200 °C, (iii) 300 °C, and (iv) 400 °C.

Table 2
The percentage presence of the Mo^{6+} and Mo^{5+} oxidation states as determined by XPS along with the work function and valence band determined via UPS for the different Molybdenum Oxide/precursor films.

Process	Mo^{6+}	Mo^{5+}	Average oxidation state	Work function (eV)	Valence band (eV)
Vacuum evaporated	94.6	5.6	$MoO_{2.97}$	−5.3	−8.10
Spray-cast, unannealed	98.5	1.5	$MoO_{2.99}$	−5.15	−8.00
Spray-cast, 200 °C	98.8	1.2	$MoO_{2.99}$	−5.10	−8.11
Spray-cast, 300 °C	87.9	12.1	$MoO_{2.94}$	−5.17	−8.17
Spray-cast, 400 °C	92.2	7.8	$MoO_{2.96}$	−5.15	−8.14

annealed at a temperature $\geqslant$300 °C. Such states are formed as a result of the thermal decomposition of Mo^{6+}. Previous work has shown that Mo^{5+} states do not have a detrimental effect upon the performance of OPVs based on organic materials having a deep HOMO level [27]. For comparison, we have also performed photoelectron spectroscopy on a MoOx film that was deposited by vacuum evaporation. It can be seen that the average oxidation state

of spray-cast films annealed at a temperature $\geqslant 300\,^{\circ}C$ are very similar to that of the vacuum evaporated MoOx film.

Fig. 3b shows the evolution of nitrogen species in spray-cast precursor films as a function of annealing temperature. Note that as the Mo3*p* peak overlaps the N1*s* peak ($\leqslant$binding energies of 399 eV), the deconvolution of the nitrogen spectra in the lower energy regions is difficult [28]. Nevertheless, we find that the spectra consist of two peaks located at 399 eV and 401.7 eV that are associated with surface adsorbed nitrogen and nitrogen in the form of ammonium respectively. We find that the intensity of the 401.7 eV peak (adsorbed nitrogen) does not vary with annealing temperature, however the peak at 399 eV (ammonium) reduces in intensity from 16.8% of the total intensity of all nitrogen species (determined in an unannealed film) to 4% (of total nitrogen) in films annealed at 400 °C. The fact that the ammonium signal is much smaller than the intensity of adsorbed atmospheric nitrogen suggests that the annealing process efficiently converts the ammonium molybdate tetrahydrate to MoOx. This finding is in accordance with previous work in which it has been demonstrated that the thermal annealing of ammonium molybdate tetrahydrate leads to its thermal decomposition and the degradation of the molybdate from Mo_7O_{24} to pure Molybdenum (VI) Oxide (MoOx) through a series of steps [29].

Fig. 3c plots UPS spectra of the precursor films that have been annealed at different temperatures. Again, we record the work-function and valence-band edge determined as a result of the UPS measurements in Table 2. It can be seen that both the secondary electron cut off and the valence band edge remain constant at (-5.13 ± 0.1) eV and (2.96 ± 0.1) eV below the Fermi level respectively. It can be seen that within experimental error, the work function and the valence band positions are identical for all films studied (including the film prepared by vacuum evaporation). This suggests that as the films are annealed, the main processes that occur are the removal of nitrogen and a limited decomposition of Mo^{6+} states into Mo^{5+}.

To explore the effect of thermal annealing on film structure, we used in situ dynamic spectroscopic ellipsometry to record changes in thickness as spray-cast ammonium molybdate tetrahydrate films as they are thermally annealed. Fig. 4 shows the thickness evolution of a ammonium molybdate tetrahydrate film as it is heated to 300 °C and subsequently cooled to room temperature. It can be seen that over the course of the entire annealing cycle the film undergoes a contraction in thickness. At temperatures below 150 °C we believe that the reduction in thickness results from the removal of residual quantities of the casting solvents acetonitrile and water that have boiling points of 82 °C and 100 °C respectively. At temperatures above 150 °C, the further contraction in film thickness most likely result from a reduction of free volume caused by a rearrangement of MoOx clusters and thermal decomposition to a material having a higher molybdenum fraction. After completion of the thermal annealing process, we find that the overall thickness of the film has been reduced by 42%, going from 13.2 to 7.7 nm. This indicates that a significant fraction of the spray-cast precursor film in fact consisted of trapped casting solvent and associated free volume. The thermal annealing cycle thus removes

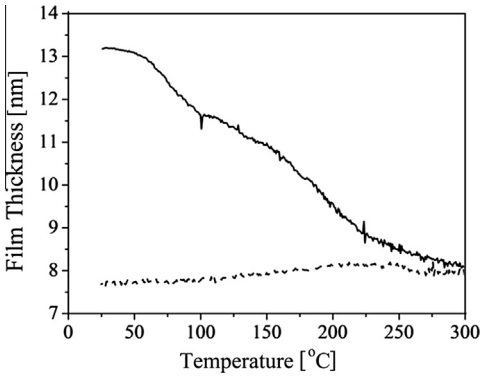

Fig. 4. The change in film thickness of a spray-cast ammonium molybdate tetrahydrate film as it is heated to 300 °C (–) and then cooled back to room temperature (■) as determined using spectroscopic ellipsometry.

casting solvent, drives the conversion of the precursor to MoOx and reduces free-volume in the film, forming a more densely packed material.

The surface profile of MoOx precursor films were studied using AFM and optical interferometry to see how the process of annealing affected the physical structure of the deposited layers over small and large scales. Fig. 5 shows 20 μm × 20 μm AFM scans for an unannealed sample (a), and samples thermally annealed at 200 °C, 300 °C and 400 °C for 1 min ((b), (c), and (d) respectively). Optical interferometry scans are shown in (e) for as sprayed films. It can be seen that over an area of $(0.46 \times 0.62)\,mm^2$ We find that the surface of the unannealed film has an RMS roughness of 0.8 nm; a value that on annealing at 200 °C and 300 °C increases to 1.4 nm and 1.6 nm respectively. In the film annealed at 400 °C we observe the formation of apparently crystalline regions together with a significant increase in RMS roughness to 6.9 nm. The uniformity of films over larger areas than the droplet size was determined through optical interferometry, it can be seen that over a $(0.46 \times 0.62)\,mm^2$ area that the surface roughness is as low as 9 nm indicating that the film has high uniformity. This would indicate that upon spraying of the solution a continuous wet film is formed. Crystallinity is confirmed using GIWAXS as shown in Fig. 6, where we plot scattering data recorded for an as-cast precursor film and a film annealed at 400 °C in parts (a) and (b) respectively. It can be seen that the as-cast film is characterised by a single broad scattering ring, corresponding to an average *d*-spacing of 0.80 nm. On annealing, the scattering pattern is characterised by a series of arc-like features corresponding to characteristic *d*-spacings of 0.71 nm and 0.33 nm out-of-plane, 0.35 nm in-plane and 0.30 nm off-axis. The form of the scattering pattern is consistent with a polycrystalline film in which there is partial order of the crystalline-planes, with the width of the scattering features corresponding to an average coherence length (domain size) on the order of 10 nm.

4. Discussion and conclusions

Our OPV device studies demonstrate a strong dependence on the temperature used to anneal the MoOx

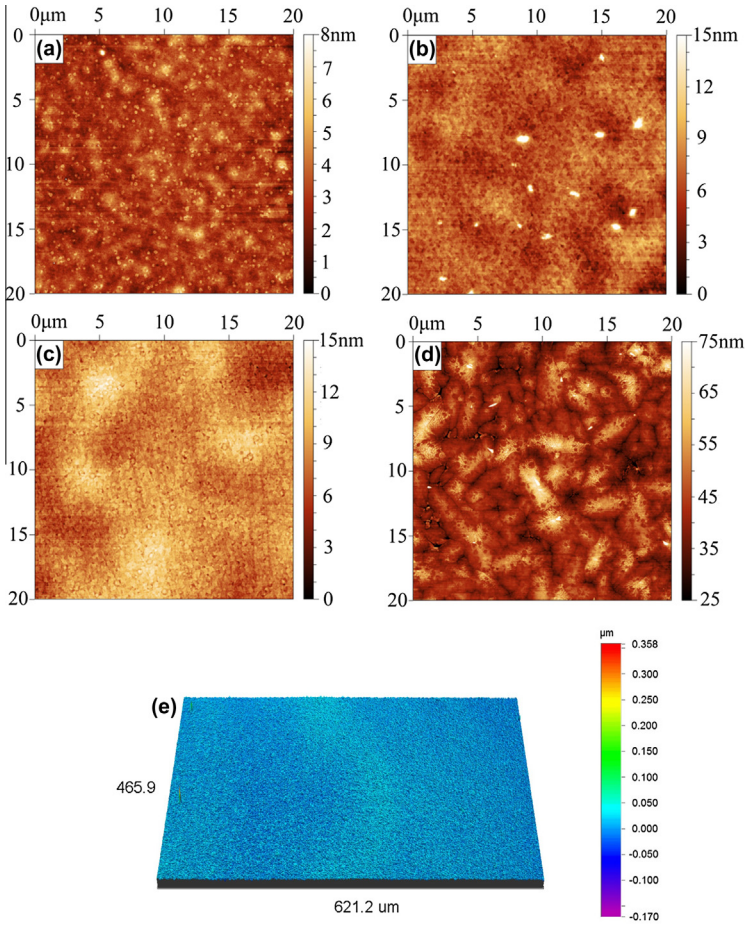

Fig. 5. Surface profile scans of the deposited films are shown. 20 μm × 20 μm AFM scans of deposited ammonium molybdate tetrahydrate films showing the surface profile for (a) unannealed films and films annealed at (b) 200 °C, (c) 300 °C and (d) 400 °C. In addition (e) shows an optical interferometry scan for an as deposited film.

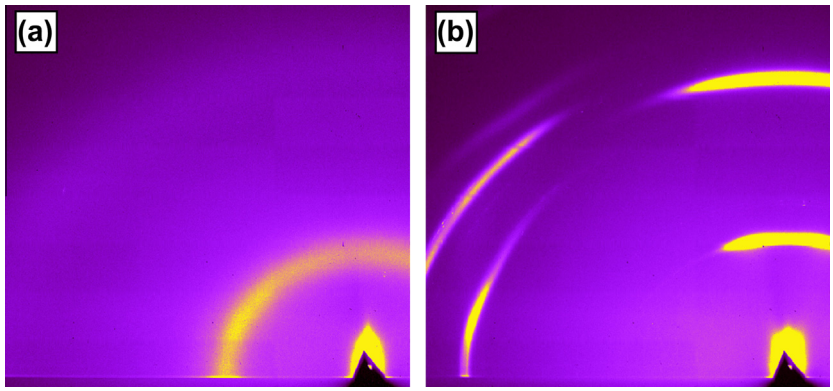

Fig. 6. GIWAXS images for ammonium molybdate tetrahydrate films (a) as cast and (b) after annealing at 400 °C.

precursor film, with a maximum PCE of 4.4% achieved at an annealing temperature of 350 °C. Previous work has shown that at 350 °C, the decomposition of ammonium molybdate tetrahydrate into molybdenum (VI) oxide is complete [29]. This result is in accord with our XPS measurements on precursor films annealed at 400 °C, in which it was found that the ammonium signal was much smaller than that of adsorbed atmospheric nitrogen. Our measurements also showed that on annealing of the precursor at 300 °C, there was a limited decomposition of Mo^{6+} states into Mo^{5+}. Our UPS measurements suggested however that the work function and the valence band positions are not

apparently sensitive to annealing temperature. We believe therefore that for films annealed at a temperature <350 °C, the poor device performance results from residual solvent that remains within the precursor film, and on the basis of our ellipsometry measurements we speculate that the ammonium and water contained within the unannealed ammonium molybdate tetrahydrate films form a resistive layer that blocks the transport and extraction of charge. This conclusion is supported by the high values for series and shunt resistance determined from the JV curve for the device containing the unannealed precursor film. Here, the poor transport of charges through the unannealed film can be attributed to the increased spatial separation of the Mo4d orbitals in molybdate precursor that act as charge transfer sites. This increased separation would likely impede transport of charge through the film via a reduction of the hopping rate. Indeed charge transfer is often problematic even in pure MoOx films, with ultra-thin films (<10 nm) generally required to achieve efficient OPV operation; a feature that derives from the insulating nature of MoOx [25]. We believe therefore that the reduction in series resistance (see Table 1) and removal of trapped solvent (see Fig. 4) in the active layer upon annealing MoOx precursor films at a temperature >200 °C contributes strongly to the observed improvements in device efficiency. However, it is possible that changes in the vertical composition of the active layer driven by the relative surface energy of the substrate (so-called vertical stratification) also occurs when films are cast onto MoOx films that have been annealed at different temperatures. Here, the exact composition of the film towards the electrode interface is known to modify charge extraction efficiency and thus impact on device performance.

For annealing temperatures above 350 °C we observed a reduction in device efficiency. Here AFM measurements demonstrated that this temperature correlates with an increased roughness of the MoOx layer. We anticipate that the asperities formed are likely to be problematic in an OPV device as they exhibit variations in peak height (~75 nm) that exceed the thickness of the active layer (60 nm) and will lead to the formation of pinholes, or otherwise cause a short-circuit. Such effects are consistent with the observed reduction in OPV shunt resistance and *FF*.

We believe that high temperatures required in order to obtain optimum device efficiency can be reduced using a number of different techniques. Indeed, our preliminary measurements suggest that annealing temperature can be reduced through reduction in precursor film thickness, with ultra-thin films (few nm) require little or no thermal annealing to produce efficient devices. The origin of this reduced necessity for annealing ultra-thin films is not as yet understood, however we note that films that have not been annealed are likely to contain a significant quantity of trapped moisture and will thus contribute to reduced device stability. More practically therefore, we note that recent work has shown that the use of self-energy combustion chemistry techniques in which the addition of an oxidiser and a fuel can be used to reduce the annealing temperature required for conversion of a precursor layer [30]. Alternatively, the use of pulsed laser irradiation has been widely used to anneal oxide films in a process fully compatible with roll-to-roll deposition onto flexible plastic substrate carrier films, with the pulsed laser minimising the heat absorbed by the underlying substrate [31]. It will be interesting to see whether such techniques can be effectively combined with the spray-cast precursor materials explored here.

5. Summary

Ultrasonic spray-coating has been used to deposit MoOx from an ammonium molybdate tetrahydrate precursor material that is then spray-cast with a PCDTBT:$PC_{71}BM$ active layer to create an organic photovoltaic device. We find that the efficiency of the organic photovoltaic device is dependent on the temperature used to anneal the precursor film, with an maximum device PCE of 4.4% achieved using an anneal temperature of 350 °C. We show that the thermal anneal process removes trapped solvent and ammonium from the film; a process that is accompanied by structural rearrangement and the chemical conversion of the precursor to MoOx. Analysis of the films using XPS and UPS reveal a small increase in Mo^{5+} states in the MoOx film; an effect that is accompanied by the loss of NH_4^+ from the layer. However annealing the film beyond around 350 °C results crystallization of the MoOx layer, forming a film having a high-surface roughness. This results in a sharp reduction in OPV PCE (caused by lower V_{oc}, *FF* and J_{sc}); a process that may result from short-circuits within the device.

Acknowledgments

We thank Claire Hurley at the Sheffield surface analysis centre for the operation and maintenance of the XPS and UPS instruments. We also thank Dr. Alan Dunbar and Mr. Tom Glen for assistance with GIWAXS measurements. We also acknowledge the UK EPSRC for funding the projects 'Transition metal oxide hole injection layers for polymer organic electronic devices' (EP/H049452/1) and 'Polymer fullerene photovoltaic devices: New materials and innovative processes for high-volume manufacture' (EP/I02864/1) and 'Supersolar Solar Energy Hub' (EP/J017361/1). Andrew Pearson would like to thank King Abdulaziz University for financial support under Grant No. D-004/431.

References

[1] B. Kippelen, Energy Environ. Sci. 2 (2009) 251.
[2] C.J. Brabec, Sol. Energy Mater. Sol. Cells 83 (2004) 273.
[3] Z. He, C. Zhong, S. Su, M. Xu, H. Wu, Y. Cao, Nat. Photonics 6 (2012) 591.
[4] A.J. Heeger, Chem. Soc. Rev. 39 (2010) 2354.
[5] B. Azzopardi, C.J.M. Emmott, A. Urbina, F.C. Krebs, J. Mutale, J. Nelson, Energy Environ. Sci. 4 (2011) 3741.
[6] S. Wakim, S. Beaupré, N. Blouin, B. Aich, S. Rodman, R. Gaudiana, Y. Tao, M. Leclerc, J. Mater. Chem. 19 (2009) 5351.
[7] H. Yi, S. Al-Faifi, A. Iraqi, D.C. Watters, J. Kingsley, D.G. Lidzey, J. Matter Chem. 21 (2011) 13649.
[8] J. Hou, Z. Tan, Y. Yan, Y. He, C. Yang, Y. Li, J. Am. Chem. Soc. 128 (2006) 4911.
[9] G. Greczynski, T. Kugler, M. Keil, W. Osikowicz, M. Fahlman, W.R. Salaneck, J. Electron. Spectro. Relat. Phenom. 121 (2001) 1.

[10] E.L. Ratcliff, J. Meyer, K.X. Steirer, N.R. Armstrong, D. Olson, A. Kahn, Org. Electron. 13 (2012) 744.
[11] H.L. Yip, A.K.Y. Jen, Energy Environ. Sci. 5 (2012) 5994.
[12] K. Zilderberg, J. Meyer, T. Riedl, J. Mater. Chem. C 1 (2013) 4796.
[13] V. Shrotriya, G. Li, Y. Yao, C. Chu, Y. Yang, Appl. Phys. Lett. 88 (2006) 073508.
[14] T. Wang, N.W. Scarratt, H. Yi, A.D.F. Dunbar, A.J. Pearson, D.C. Watters, T.S. Glen, A.C. Brooks, J. Kingsley, A.R. Buckley, M.W.A. Skoda, A.M. Donald, R.A.L. Jones, A. Iraqi, D.G. Lidzey, Adv. Energy Mater. 3 (2013) 505.
[15] D.C. Watters, J. Kingsley, H. Yi, T. Wang, A. Iraqi, D.G. Lidzey, Org. Electron. 13 (2012) 1401.
[16] W. Nie, R.C. Coffin, J. Liu, E.D. Peterson, C.M. MacNeill, R.E. Noftle, D.L. Carroll, Appl. Phys. Lett. 100 (2012) 083301.
[17] G. Susanna, L. Salamandra, T.M. Brown, A.D. Carlo, F. Brunetti, A. Reale, Sol. Energy Mater. Sol. Cells 95 (2011) 1775.
[18] J.G. Tait, B.P. Rand, P. Heremans, Org. Elecron. 1002 (2013) 14.
[19] C. Girotto, D. Moia, B.P. Rand, P. Heremans, Adv. Funct. Mater. 21 (2011) 64.
[20] J.B. Mooney, S.B. Radding, Ann. Rev. Mater. Sci. 12 (1982) 81.
[21] K. Zilberberg, H. Gharbi, A. Behrendt, S. Trost, T. Riedl, ACS Appl. Mater. Interfaces 4 (2011) 1164.
[22] J.J. Jasieniak, J. Seifter, J. Jo, T. Mates, A.J. Heeger, Adv. Funct. Mater. 22 (2012) 2594.
[23] S.R. Hammond, J. Meyer, N.E. Widjonarko, P.F. Ndione, A.K. Sigdel, A. Garcia, A. Miedaner, M.T. Lloyd, A. Khan, D.S. Ginley, J.J. Berry, D.C. Olson, J. Mater. Chem. 22 (2012) 3249.
[24] C. Girotto, E. Voroshazi, D. Cheyns, P. Heremans, B.P. Rand, ACS Appl. Mater. Interfaces 3 (2011) 3244.
[25] S. Murase, Y. Yang, Adv. Mater. 24 (2012) 2459.
[26] T. Wang, A.J. Pearson, A.D.F. Dunbar, P.A. Staniec, D.C. Watters, H. Yi, A.J. Ryan, R.A.L. Jones, A. Iraqi, D.G. Lidzey, Adv. Funct. Mater. 22 (2012) 1399.
[27] J. Griffin, D.C. Watters, H. Yi, A. Iraqi, D.G. Lidzey, A.R. Buckley, Adv. Energy. Mater. 3 (2013) 903–908.
[28] D.R. Lide, Handbook of Chemistry and Physics, CRC Press, Bocan Raton, FL, USA, 1998.
[29] W.M. Shaheen, M.M. Selim, J. Therm. Anal. Calorim. 59 (2000) 961–970.
[30] M.G. Kim, M.G. Kanatzidis, A. Facchetti, T.J. Marks, Nat. Mater. 10 (2011) 382.
[31] E.D. Tsagarakis, C. Lew, M.O. Thompson, E.P. Giannelis, Appl. Phys. Lett. 89 (2006) 202910.